PHYSICAL REVIEW A VOLUME 47, NUMBER 2 FEBRUARY 1993

Stark effect for the Rydberg states of the krypton atom near the ionization threshold

Kenji Ito
National Laboratory for High Energy Physics, Photon Factory, Tsukuba, Ibaraki 305, Japan

Hiroki Masuda and Yumio Morioka
University of Tsukuba, Institute of Physics, Tsukuba, Ibaraki 305, Japan

Kiyoshi Ueda
Tohoku University, Research Institute for Scientific Measurements, Sendai 980, Japan
(Received 13 August 1992)

We have measured the Stark effect on absorption spectra of highly excited Rydberg levels near the ionization threshold of Kr. The spectra were recorded against the continuum from a synchrotron-radiation (SR) light source using a high-resolution vacuum-ultraviolet spectrometer and applying electric fields that were parallel or perpendicular to the polarization of the SR. The main features are hydrogen-like Stark manifolds that arise from mixing of high-orbital-angular-momentum states with negligible quantum defects, and a number of lines belonging to the *np* and *nd* ($J=2$) series, the appearance of the latter being strongly dependent on the direction of the external field with respect to the SR polarization. Based on the diagonalization of the Stark energy matrix including more than 450 configurations, the *np* and *nd* ($J=2$) series are correlated with the zero-field states. The term values of the zero-field states are obtained by extrapolation of observed energy values to the zero electric field. A multichannel-quantum-defect-theory analysis has been carried out for the $J=1$ even-parity energy levels to derive the eigenchannel quantum defects and transformation matrix elements.

PACS number(s): 32.30.Jc, 32.60.+i

I. INTRODUCTION

Rydberg states of rare-gas atoms have received much attention from both experimentalists and theorists for many years. The absorption spectrum in the photoionization threshold region consists of five Rydberg series, and shows a typical Beutler-Fano profile [1] between the ground-state ion levels of $j=\frac{1}{2}$ and $j=\frac{3}{2}$. The energy levels of the five series have been obtained with high-resolution absorption measurements [2–6] that produced important data for theoretical analyses based on multichannel quantum-defect theory (MQDT) [7–9]. Aymar, Robaux, and Thomas [10] have systematically analyzed the $J=0$, 1, 2, and 3 energy levels of Kr I with odd parity, obtained by Delsart, Keller, and Thomas [11], Yoshino and Tanaka [3], Moore [12], and Kaufman and Humphreys [13].

Attention has recently been paid to the Stark effect of high-lying states of atoms, owing to the development of high-resolution laser spectroscopy. Modern laser techniques enable the separation of highly excited Rydberg states to be observed at electric fields of a few thousand V/cm which are easily realized in laboratory frames. Zimmerman *et al.* [14] have investigated the Stark effect on the Rydberg states of alkali-metal atoms. Harmin [15] and Sakimoto [16] have independently carried out theoretical treatments based on MQDT to interpret Zimmerman's experimental data. As for the Stark effect on the Rydberg states of heavy rare gases, few systematic investigations have been done, mainly because of insufficient tunability of laser frequencies. Ernst, Softely, and Zare [17] have investigated the Stark effect on the Xe autoionizing Rydberg series using coherent radiation generated by frequency tripling. Laser spectroscopic studies on metastable atoms were applied to the studies on the Stark structures of the Kr and Xe Rydberg series by Delsart and Keller [18], and Knight and Wang [19]. Brevet, Pellaim, and Vialle [20] have investigated the Stark effect in Ar Rydberg states using a similar laser spectroscopic technique.

We have investigated the effect of external electric fields on the Kr Rydberg series below the ionization threshold. To our knowledge, there have been do direct absorption measurements of the Stark effect in the vacuum ultraviolet (vuv) region. The homogeneous wavelength distribution of synchrotron radiation (SR) enabled us to carry out systematic measurements in wide energy regions. The high-resolution spectrometer employed in the present study is expected to produce important information for the elucidation of the correlation among various Rydberg series in the presence of an external electric field.

II. EXPERIMENT

The absorption measurements for Kr Rydberg states were carried out at the Photon Factory by using the 6VOPE facility, which consists of a 6.65-m vertical dispersion off-plane Eagle spectrometer and a zero-dispersion tandem concave grating predisperser [21]. Synchrotron radiation from a 2.5-GeV positron storage ring was used as a background source.

An absorption cell of 16.5-cm length was installed in a vacuum chamber between the predisperser system and the main spectrometer. The absorption cell consists of two parallel plates of aluminum and insulating material. High voltage (0–2 kV) was applied to one plate and the other was grounded. The distance between the two plates was 5 ± 0.1 mm along the light path. Inhomogeneities in the electric field might affect spectral profiles; however, as shown below, a notable effect on observed spectral lines was not recognized. Two apertures (2 mm in diameter) were made for the incident light to enter and exit the absorption cell. Krypton gas supplied from Teisan Co., LTD. (purity $\geq 99.99\%$) was used without any purification. The sample gas pressure in the absorption cell was estimated to be 0.5–0.05 Torr.

Absorption spectra were registered on Kodak short-wavelength radiation plates by employing the spectrograph mode of the 6VOPE facility in the sixth spectral order of a 1200-lines/mm grating. The resolving power of the facility was estimated to be $\approx 2.5\times10^5$ in this spectral region [21]. It is useful to recall that the Doppler line broadening is $\approx 1\times10^{-3}$ Å ($0.15\ \mathrm{cm}^{-1}$) for the absorption spectral lines of Kr Rydberg states. Typical exposure times were 10–20 min, which were ten times longer than usual exposure times because of the two limiting apertures. To provide comparison lines for the wavelength determination, emission lines of the CO fourth positive bands in the third spectral order were superimposed on the sixth-order absorption spectrum of Kr [6,22]. A small amount of Ar was introduced into the spectrometer in order to record the $3d[1/2]_1$ absorption line (894.3132 Å [23]) along with Kr absorption for an absolute wavelength determination. Photographic plates were measured with a Grant Instruments spectral line comparator at the Harvard-Smithsonian Center for Astrophysics. The absolute wavelength accuracy of measured spectral lines was estimated to be less than 2×10^{-3} Å ($0.3\ \mathrm{cm}^{-1}$) from the uncertainty ($\approx 1\ \mu$m) in measuring the absolute positions of spectral lines with the comparator.

III. RESULTS AND DISCUSSION

A. General features of observed spectra

Densitometer traces for absorption spectra of Kr Rydberg states are shown in Figs. 1 and 2 for different electric fields. The direction of the electric field is parallel and perpendicular to the polarization of incident exciting light, respectively, for Figs 1 and 2. At zero electric field, two strong and one weak series are seen; the strong are identified as $ns[3/2]_1$ and $nd[3/2]_1$ series and the weak series as $nd[1/2]_1$. These three series are known to converge to the first ionization limit $^2P_{3/2}$ Kr^+. The perturbation to the Coulomb potential by the applied electric field E forms a potential barrier, which classically reduces the ionization threshold by $2\sqrt{E}$. Critical-field-ionization thresholds are shown by arrows corresponding to the applied fields in Figs. 1 and 2. It is worthwhile to point out that the observed spectra do not show a simple continuum beyond the critical ionization threshold. Although the photographic detection does not always give quantitative information for absorption intensities, the energy region where the spectra show rich structures beyond the field-ionization threshold seems to increase

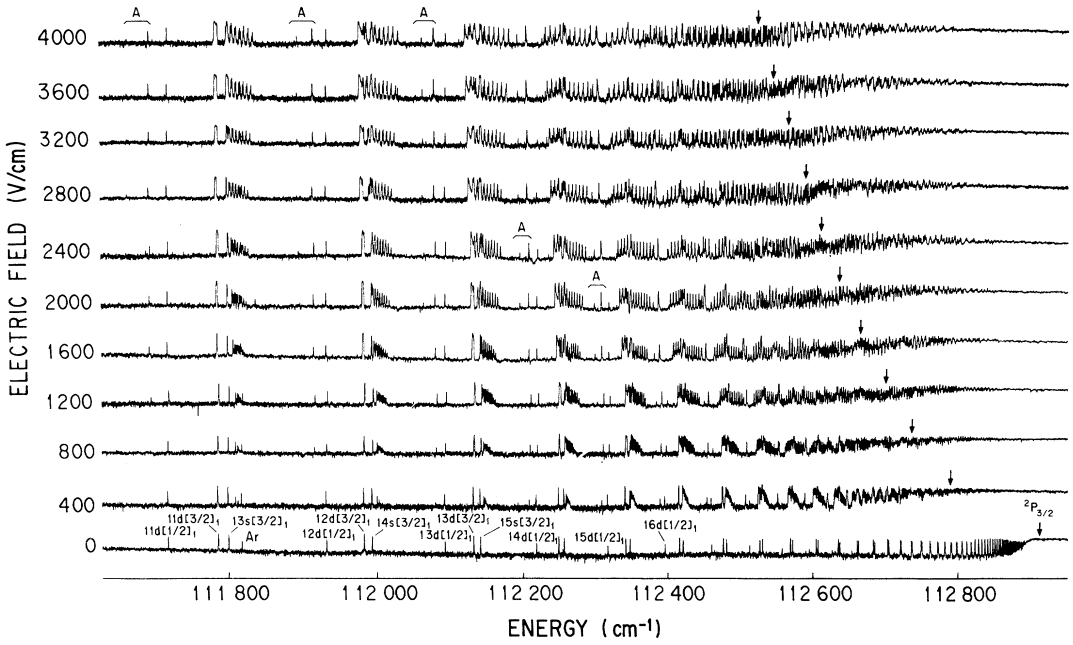

FIG. 1. Densitometer trace of Kr I Stark absorption spectra near the ionization threshold. The direction of applied field was parallel to the polarization of the SR. The critical fields for ionization are shown by arrows for each field strength. The *np* series, indicated by *A*, appear in the long-wavelength side of the $nd[1/2]_1$ series (see text).

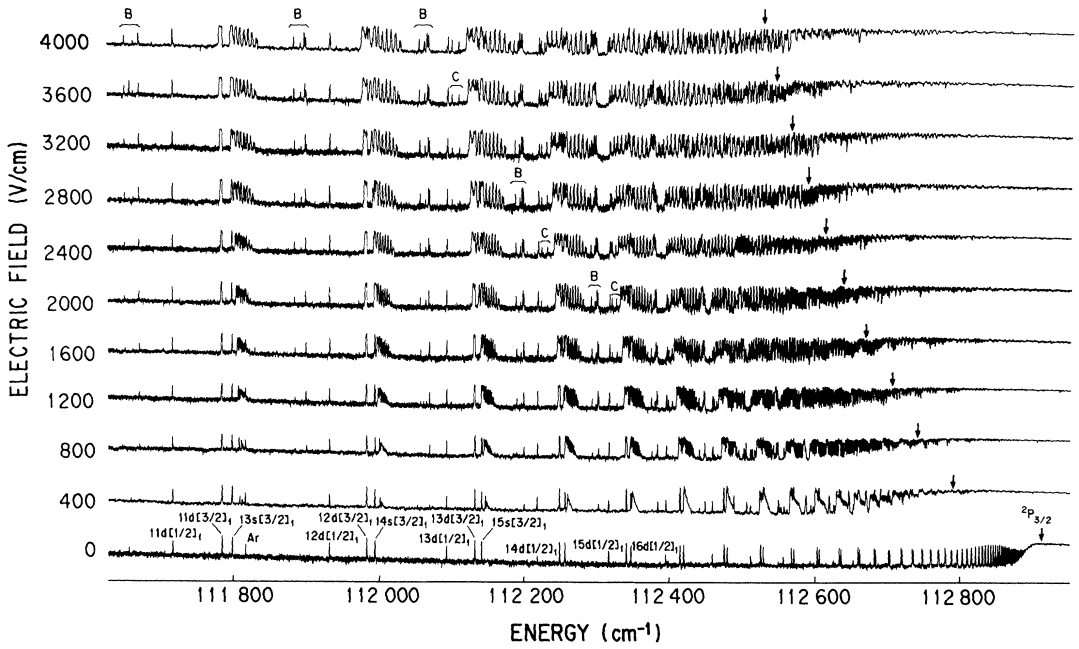

FIG. 2. Densitometer trace of Kr I Stark absorption spectra near the ionization threshold. The direction of applied field was perpendicular to the polarization of the SR. The critical fields for ionization are shown by arrows for each field strength. The *np* and $nd(J\neq 1)$ series, indicated by *B* and *C*, respectively, appear with increasing electric fields (see text).

with increasing applied electric field. The contribution of the centrifugal potential plays an important role for the energy levels with large orbital angular momentum and results in the existence of discrete energy levels beyond the critical field-ionization potential.

Absorption lines other than the three Rydberg series appear under the applied electric field. Some remarkable points, which are seen in Figs. 1 and 2, will be discussed below.

A few absorption lines, which are indicated by *A* and *B* in Figs. 1 and 2, respectively, appear clearly in the longer-wavelength side of the $nd[1/2]_1$ lines under the electric field. These spectral lines increase their absorption intensities and are shifted to longer wavelengths with increasing electric field. These spectral lines are apparently periodic except for the energy region close to the ionization threshold, and form some Rydberg series. Two Rydberg series (*A*) are seen in Fig. 1, where the polarization of the incident light is parallel to the applied field. In the case where the polarization is perpendicular to the field (Fig. 2), four Rydberg series (*B*) are seen. The higher members of the Rydberg series are easily seen at relatively low electric fields; however, some of the members lying on the longer wavelength side of the $9d[1/2]_1$ line are not seen at a field strength of 4000 V/cm. This tendency reflects the fact that the higher energy level is very sensitive to the effect of the applied field. These absorption lines might be caused by the transitions from the ground state Kr $^1S_0$ to the energy levels which are strongly coupled to the Rydberg series appearing at zero field. These spectral lines might be temporarily assigned to the *np* series judging from the quantum defects: the decimal parts of the quantum defects lying between 0.5 and 0.7.

The absorption intensity of the $nd[1/2]_1$ series apparently becomes weak at higher electric fields. Furthermore, the spectral position seems to be independent of the field strength, contrary to the *np* series.

Another periodic feature, consisting of two Rydberg series, is seen at the shorter-wavelength side of the $nd[1/2]_1$ series in Fig. 2, where the polarization is perpendicular to the electric field. These two series are indicated by *C* in Fig. 2. Absorption of these two series is relatively weak in comparison with the *np* series. These Rydberg series are temporarily assigned to the *nd* series with $J\neq 1$ based on their quantum defects. As in the case of *np* series, the spectral lines of the $nd(J\neq 1)$ series shift to the longer-wavelength side, and the higher members have a tendency to appear strongly at low electric fields.

The most beautiful feature in the Stark absorption spectra is the hydrogenlike Stark manifold caused by the mixing of *l* states with very small quantum defects [$l=3$ to $(n-1)$]. The enlarged trace of the absorption spectra are shown in Figs. 3 and 4, respectively, for the polarization parallel and perpendicular to the applied field. The Rydberg series marked *A*, *B*, and *C* are the same as those indicated in Figs. 1 and 2. Contrary to the isolated absorption of the *np* and $nd(J\neq 1)$ series, the Stark manifold shows no remarkable dependence on the direction of the polarization. At low electric fields, where the $ns[3/2]_1$ and $nd[3/2]_1$ levels do not merge into the manifolds, the manifolds are composed of $n-3$ members because the *ns*, *np*, and *nd* levels have large quantum defects. The higher members of the $ns[3/2]_1$ and $nd[3/2]_1$ series merge into the manifolds at relatively low electric fields; the $16d[3/2]_1$ merges by 800 V/cm, while the

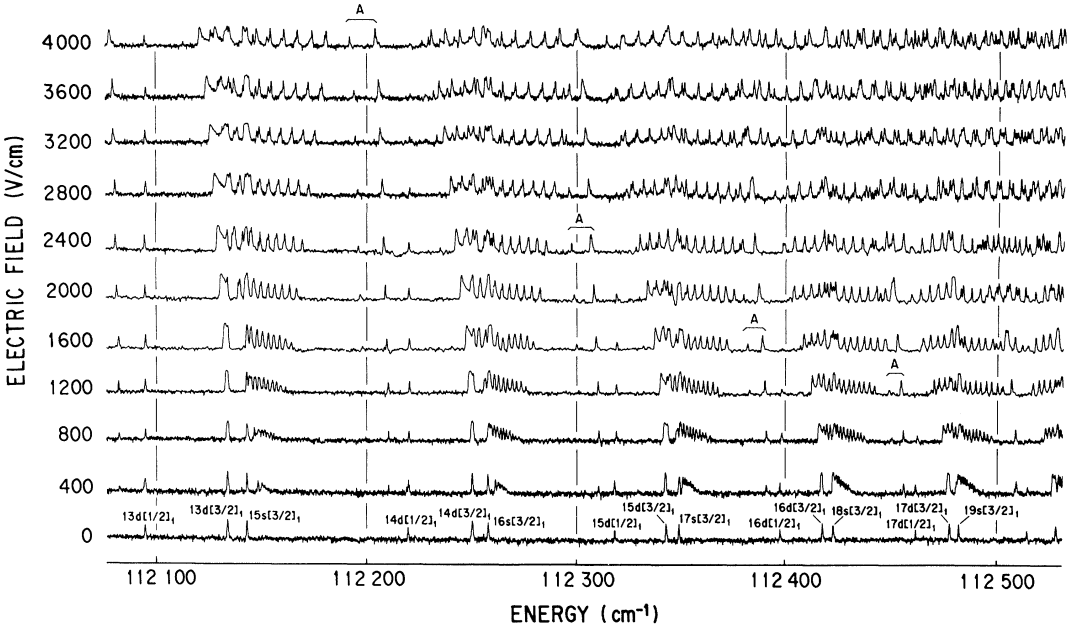

FIG. 3. Enlarged densitometer trace of Kr I Stark absorption spectra shown in Fig. 1. The series with A are the same as in Fig. 1.

$14d[3/2]_1$ merges by 1600 V/cm. The present manifolds do not show the simple structures such as those obtained for alkali-metal atoms [14], Xe [17,19], and Ar [20], even at sufficiently low electric fields where the anticrossing between two different manifolds does not begin. The splitting between the linear manifold components seems to be dependent of the field strength where the $ns[3/2]_1$ does not merge into manifold, and the intensity of the components decreases systematically with increasing wave number. However, at a higher field where the $ns[3/2]_1$ and $nd[3/2]_1$ levels merge into the manifold, there are manifold components with two or three subcomponents or with a distorted spectral profile. The $n^{0.7}$ dependence of the splitting between manifolds has been reported [17,18]. However, we were unable to obtain such a relation from the present data.

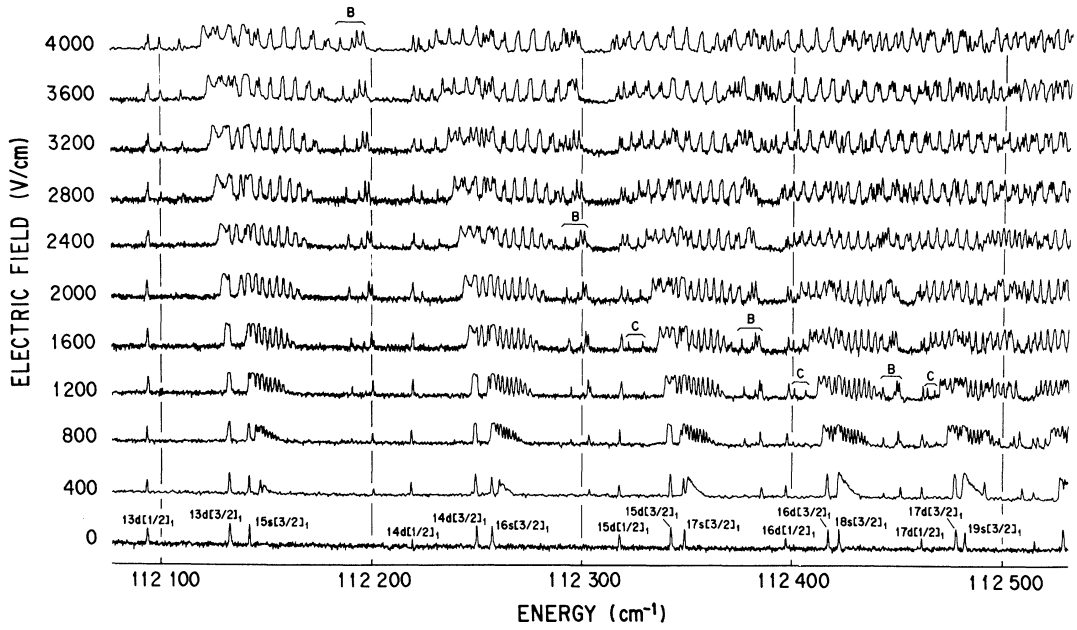

FIG. 4. Enlarged densitometer trace of Kr I Stark absorption spectra shown in Fig. 2. The series with B and C are the same as in Fig. 2.

B. Simulation of Stark spectra

The simulation of the Stark spectra was carried out for a better understanding of the observed spectra. Although there are strict theoretical treatments for the effect of external electric fields on absorption spectra of alkali atoms and also more general atoms based on the multichannel quantum-defect theory [15,16], the diagonalization method of the Stark energy matrix was adopted in the present report for the simulation. This method has already been applied to the simulation of Xe spectra [17,19] and Ar spectra [20], and will be described briefly in the following paragraph.

The *jl*-coupling basis scheme is used to described the Kr Rydberg series. The strong coupling of the orbital angular momentum of the Rydberg electron l to the ion-core total angular momentum $\mathbf{j}$ results in an angular momentum of $\mathbf{K}=\mathbf{j}+l$. The resultant $\mathbf{K}$ is weakly coupled to the Rydberg electron spin $\mathbf{s}$. We then get the total angular momentum of the whole system $\mathbf{J}=\mathbf{K}+\mathbf{s}$. The *jl*-coupling basis function is written as $nl[K]_J$, and is an eigenfunction of the zero-field Hamiltonian H_0. The Stark Hamiltonian under the applied electric field is described as $H=H_0+eEz$. The diagonal elements for the Stark energy matrix are obtained from the experimental values. For the Rydberg series of which higher members ($n>10$) have not been measured, the quantum defects are derived by extrapolating the lower members of the series. The quantum defects for Rydberg series used in the present simulation are listed in Table I. The quantum defects for the Rydberg series with high orbital angular momentum ($l>3$) are assumed to be zero.

The off-diagonal element of the Stark energy matrix is described as

$$\langle (\nu lj)KsJM|z|(\nu' l' j')K' s' J' M'\rangle = (-1)^{J+J'+K+K'+l+j+s-M}[(2J+1)(2J'+1)(2K+1)(2K'+1)]^{1/2} \times \begin{pmatrix} J & 1 & J' \\ -M & 0 & M \end{pmatrix} \begin{Bmatrix} K & J & s \\ J' & K' & 1 \end{Bmatrix} \begin{Bmatrix} l & K & J \\ K' & l' & 1 \end{Bmatrix} \langle \nu l \| r \| \nu' l' \rangle , \quad (1)$$

TABLE I. Quantum defects for the nl series used in the simulation. Columns 3–7 give the n values of observed levels.

Level	Quantum defect	Ref. [13]	Ref. [12]	Ref. [3]	Ref. [11]	Ref. [25]
$ns[3/2]_1$	3.08	5–10	5–12	5–33		
$ns[3/2]_2$	3.10	5–10	5–12			
$np[1/2]_0$	2.52	5–8	5–11			19–49
$np[1/2]_1$	2.67	5–8	5–10			19–45
$np[3/2]_1$	2.60	5–8	5–9			
$np[3/2]_2$	2.59	5–8	5–10			19–32
$np[5/2]_2$	2.63	5–7	5–9			
$np[5/2]_3$	2.63	5–8	5–9			
$nd[1/2]_0$	1.46	4–9	4–11			
$nd[1/2]_1$	1.45	4–9	4–8,10,11	4–29	24–35	
$nd[3/2]_1$	1.15	4–8	4–9,12,13	4–60	24–45	
$nd[3/2]_2$	1.29	4–8	4–11		15–61	
$nd[5/2]_2$	1.30	4–8	4–10		24–50	
$nd[5/2]_3$	1.28	4–8	4–11		24–46	
$nd[7/2]_3$	1.35	4–9	4–12		15–53	
$nd[7/2]_4$	1.39	4–11	4–13			
$nf[3/2]_1$	0.03	4–5	4–10			16–44
$nf[3/2]_2$	0.03	4–5	4–10			16–44
$nf[5/2]_2$	0.02	4–5	4–8			
$nf[5/2]_3$	0.02	4–6	4–10			
$nf[7/2]_3$	0.01	6	4–7			
$nf[7/2]_4$	0.01	6	4–7			
$nf[9/2]_4$	0.03	5–6	5–8			
$nf[9/2]_5$	0.03	5	4–10			
nl ($l>3$)	0.00					

with

$$\langle \nu l \| r \| \nu' l' \rangle = \begin{cases} -\sqrt{l+1}\langle \nu l | r | \nu' l' \rangle, & l' = l+1 \\ \sqrt{l}\,\langle \nu l | r | \nu' l' \rangle, & l' = l-1, \end{cases} \quad (2)$$

where ν is the effective quantum number. The radial integral that appears in the right-hand side of Eq. (2) was calculated using the tables by Edmonds *et al.* [24].

The $\Delta M = 0$ transitions are allowed when the polarization of the incident light is parallel to the direction of the external electric field, while the $\Delta M = \pm 1$ selection rule is applied to the perpendicular polarization. Since $M = 0$ for the ground state of the Kr atom, pure $M = 0$ or $M = \pm 1$ can be excited for the parallel or perpendicular polarization. For $\nu = 11-15$, 480 and 470 basis functions are included in the diagonalization procedure for $M = 0$ and $M = \pm 1$. The Rydberg series with $J = 0$ should be excluded in the case of $M = \pm 1$. The eigenstate obtained from the matrix diagonalization is represented as a linear combination of the basis wave functions. The absorption intensity of the eigenstates is obtained by summing the square of the coefficients multiplied by the absorption intensity at zero field over the $ns[3/2]_1$, $nd[1/2]_1$, and $nd[3/2]_1$ series. In this simulation, we adopted the absorption intensities for these series measured by Yoshino and Tanaka [3]. The results of the present simulation for an applied field of 2000 V/cm are shown together with the observed spectra in Fig. 5. In the simulated spectra are shown the energy levels and the absorption intensities. The present simulation properly reproduces the spectral line positions in the observed spectra. However, the absorption intensities in the simulation are not always in agreement with those in the observed spectra. It should be pointed that it is generally difficult to obtain absolute absorption intensities from photographic measurements. However, since we are mostly interested in the assignment of the *np* and $nd(J \neq 1)$ series, the simple model in the present simulation is useful in the following discussion in spite of the insufficient results on the absorption intensities.

The eigenstates obtained by the diagonalization method are represented by the linear combination (LC) of the *jl*-coupling basis set. The LC coefficient of one basis function is always predominant for the electric fields used in the present measurements except for the spectral lines in the Stark manifolds. The observed spectral lines are characterized by the predominant LC coefficients and are given the assignments which are shown in Fig. 5.

Three *np* series appear in the simulated spectra for $M = 0$; the strongest $np[1/2]_0$, $np[5/2]_2$, and the weakest $np[3/2]_2$. The weakest series was not observed in the present measurement. The simulated intensity ratio for the three series is in good agreement with the measurements. The Stark selection rules in *jl*-coupling are

$$\Delta M = \Delta S = \Delta j = 0\ ,$$
$$\Delta J = \pm 1 \ \text{ for } M = 0\ , \quad \Delta J = 0, \pm 1 \ \text{ for } M = \pm 1\ , \quad (3)$$
$$\Delta K = 0, \pm 1, \quad \Delta l = \pm 1\ .$$

The $np[1/2]_0$ series can be coupled to the $nd[1/2]_1$ and $nd[3/2]_1$ series. The simulation, however, shows the preference of the $nd[1/2]_1$ series lying closer to the $np[1/2]_0$ series. The $np[5/2]_2$ series is found to be coupled to the $ns[3/2]_1$ rather than to the $nd[3/2]_1$ in the simulation, though the $nd[3/2]_1$ state is located much closer to the $np[5/2]_2$ state than the $ns[3/2]_1$ state.

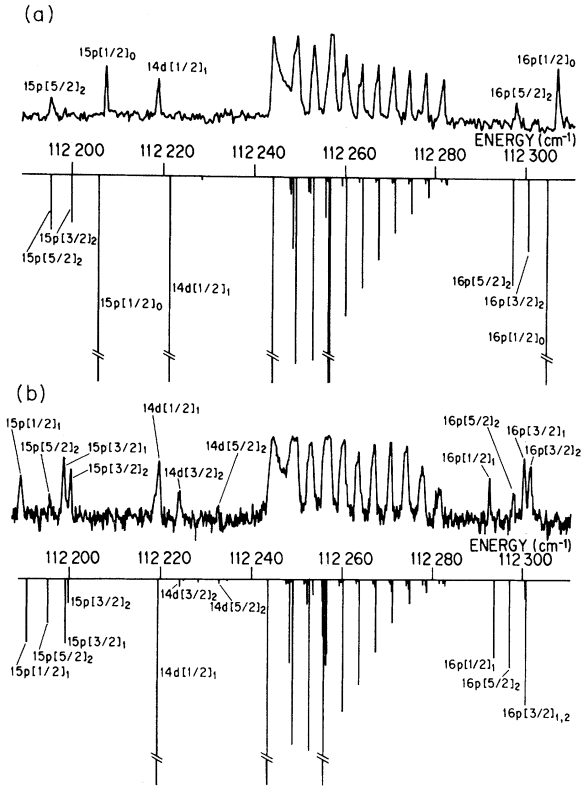

FIG. 5. Densitometer traces of the observed and simulated spectra for (a) $M = 0$ and (b) $M = \pm 1$ observed at an electric field of 2000 V/cm. The assignments for the spectral lines are deduced from the Stark matrix diagonalization method (see text).

For the $M = \pm 1$ case, four *np* series are seen in the observed spectra: three strong $np[3/2]_1$, $np[3/2]_2$, $np[1/2]_1$ series and one weak $np[5/2]_2$ series. The simulation does not show a strong absorption for the $np[3/2]_2$ series; however, there is qualitative agreement between the simulated and the observed spectra. Based on the simulation, the $np[3/2]_2$ and $np[1/2]_1$ series are coupled to the $nd[1/2]_1$ series, and the $np[5/2]_2$ series is coupled to the $ns[3/2]_1$ series. The $np[3/2]_1$ series is exceptionally coupled to the three Rydberg series $ns[3/2]_1$, $nd[1/2]_1$, and $nd[3/2]_1$.

The $np[1/2]_0$ series exists only in the $M = 0$ spectra, for the $J = 0$ state does not have $M = \pm 1$ sublevels. The absence of the $J = 1$ series in the $M = 0$ spectra is explained in terms of the selection rules; $\Delta J \neq 0$ for $M = 0$.

The simulation suggests that the absorption intensity of the $nd[K]_J(J \neq 1)$ is too low to be observed in the $M = 0$ spectra. However, for $M = \pm 1$, two *nd* series appear both in the simulated and observed spectra; the higher level is temporarily assigned to the $nd[5/2]_2$

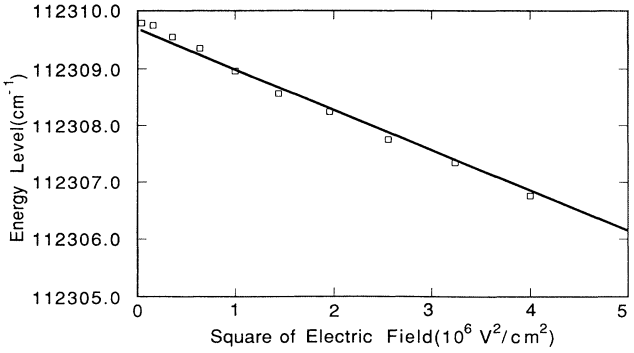

FIG. 6. The observed energy levels of the spectral line correlated with the $16p[1/2]_0$ state at zero electric field are plotted against the square of the electric field.

series, and the lower level is assigned to the $nd[3/2]_2$ or $nd[7/2]_3$ series. The Stark selection rules do not allow the direct coupling of these series to the $ns[3/2]_1$, $nd[1/2]_1$, and $nd[3/2]_1$ series, which have dipole transition moments from the ground state. The second-order coupling, for example, the $nd[5/2]_2$, is coupled to the $np[3/2]_1$, which is coupled to one of the $ns[3/2]_1$, $nd[1/2]_1$, and $nd[3/2]_1$ series, seems to be important for the appearance of $nd[K]_J(J\neq 1)$ series.

C. Energy levels of the *np* series with $J=0$ and 1 at zero field

As for the energy levels which are not energetically degenerate, the shift of the energy levels is linearly proportional to the square of the electric-field strength. In Fig. 6, the observed wave number of the $16p[1/2]_0$ state is plotted against the square of the applied field. The solid line represents a linear relation obtained by a least-squares fit, and the extrapolation to zero field gives the term value of the $16p[1/2]_0$ state. We believe that the term value deduced in this way has an uncertainty less than 0.3 cm^{-1}. In Table II, the energy levels of the $np[1/2]_0$ series in the present experiment are listed together with the previous measurements. Our energy levels are in good agreement with the values of Moore [12] and Audouards *et al.* [25] within their experimental er-

TABLE II. Energy levels for the $np[1/2]_0$ series.

n	This work	Ref. [12][a]	Ref. [25]
10	110 956.6	110 956.33	
11	111 390.2	111 390.40	
12	111 694.3		
13	111 915.6		
14	112 081.7		
15	112 209.4		
16	112 309.7		
17	112 390.1		
18	112 455.3		
19	112 508.9		112 509.1

[a]Term values reduced to take into account the correction (-0.7 cm^{-1}) of Petersson [27].

TABLE III. Energy levels for the $np[1/2]_1$ series.

n	This work	Ref. [12][a]	Ref. [13]	Ref. [25]
5		91 168.61	91 168.58	
6		102 887.30	102 887.26	
7		107 005.48	107 005.43	
8		109 082.88	109 082.84	
9		110 180.27		
10		110 872.52		
11	111 333.8			
12	111 653.5			
13	111 885.4			
14	112 058.5			
15	112 191.1			
16	112 294.9			
17	112 377.3			
18	112 443.2			
19	112 529.2[b]			112 529.7
20				112 558.1
21				112 591.2
22				112 623.1
23				112 650.6
24				112 674.4
25				112 695.3
26				112 713.6
27				112 729.6
28				112 743.9
29				112 756.6
30				112 768.0

[a]Term values reduced to take into account the correction (-0.7 cm^{-1}) of Petersson [27].
[b]Observed energy level at 50 V/cm.

TABLE IV. Energy levels for the $np[3/2]_1$ series.

n	This work[a]	Ref. [12][b]	Ref. [13]
5		92 964.49	92 964.46
6		103 313.58	103 313.53
7		107 221.44	107 221.40
8		109 149.80	109 149.76
9		110 234.94	
10	110 910.0		
11	111 360.3		
12	111 673.1		
13	111 900.4		
14	112 070.5		
15	112 201.1		
16	112 303.5		
17	112 385.1		
18	112 450.3		
19	112 509.3		
20	112 552.9		
21	112 590.9		
22	112 623.1		
23	112 651.0		
24	112 674.8		
25	112 695.8		

[a]Observed energy levels at 50 V/cm were listed for $n \geq 19$.
[b]Term values reduced to take into account the correction (-0.7 cm^{-1}) of Petersson [27].

TABLE V. Energy levels for the $7p'$ states.

Level	This work	Ref. [25]
$7p'[1/2]_0$	not determined	112 668.3
$7p'[1/2]_1$	112 497.7	112 498.1
$7p'[3/2]_1$	112 490.1	112 490.3
$7p'[3/2]_2$	112 543.6	112 543.8

TABLE VI. Eigenchannel MQDT parameters for four $J=1$ channels of Kr I.

α	1	2	3	4
μ_α	0.702 0	0.598 9	0.594 2	0.650 1
$U_{1\alpha}$	0.552 912	0.000 000	−0.791 296	−0.261 035
$U_{2\alpha}$	0.588 439	0.707 107	0.359 634	0.156 215
$U_{3\alpha}$	−0.588 439	0.707 107	−0.359 634	−0.156 215
$U_{4\alpha}$	−0.042 052	0.000 000	−0.339 378	0.939 710

ror. Audouards *et al.* [25] have measured the term values for $n=19-49$ and pointed out that in the MQDT analysis of the even-parity energy levels with $J=0$ the $np[1/2]_0$ series is strongly perturbed in the vicinity of the $7p'[1/2]_0$ state (112 668.3 cm^{-1}).

The energy levels for the $np[3/2]_1$ and $np[1/2]_1$ series, deduced as those for the $np[1/2]_0$ series, are listed in Tables III and IV, respectively, with the previous experimental measurements. These are the experimental data for these two series in the energy region of the present measurement. The enlarged absorption spectra for $M=\pm1$ are shown in Fig. 7 with applied electric fields of 0–400 V/cm. The $np[1/2]_1$ and $np[3/2]_1$ series seem to be located regularly up to $n=18$; however, they are perturbed above the energy levels of the $7p'[1/2]_1$ and $7p'[3/2]_1$ states. The $np[1/2]_1$ energy levels for $n=19$ and 20 are particularly shifted to the high-energy side, jumping over the $np[3/2]_1$ levels. The assignments for the $19p[1/2]_1$ and $20p[1/2]_1$ states are based on the measurements by Audouards *et al.* It is emphasized that the $20p[1/2]_1$ state seems to be strongly correlated with the $19d[1/2]_1$ state, which is located very close to the $20p[1/2]_1$ state at zero field. The Stark energy shift of the $19d[1/2]_1$ is >1 cm^{-1} at an electric field of 200 V/cm, whereas the energy shifts of the $17d[1/2]_1$ and $18d[1/2]_1$ are not within our experimental errors at electric fields up to 200 V/cm.

The two series with $n>21$, which may not be strongly perturbed because of their distance from the two $7p'[1/2]_1$ and $7p'[3/2]_1$ states, are expected to appear again regularly as with $n<18$. However, the np series with $n\geq21$ appear in a different way; there are at very low electric fields one strong series and one weak series which are tentatively assigned to the $np[3/2]_1$ and $np[1/2]_1$ series, respectively. The $np[1/2]_1$ series appears on the low-energy side of the $np[3/2]_1$ series except for $n=19-21$. As the electric field increases, states other than the $np[1/2]_1$ and $np[3/2]_1$ states may contribute to the observed spectra. We abandoned attempts to obtain the energy levels by extrapolation to zero field for the higher members of the np series. In Tables III and IV, the observed energy levels at 50 V/cm are listed for $n\geq19$ instead of the extrapolated values. The energy lev-

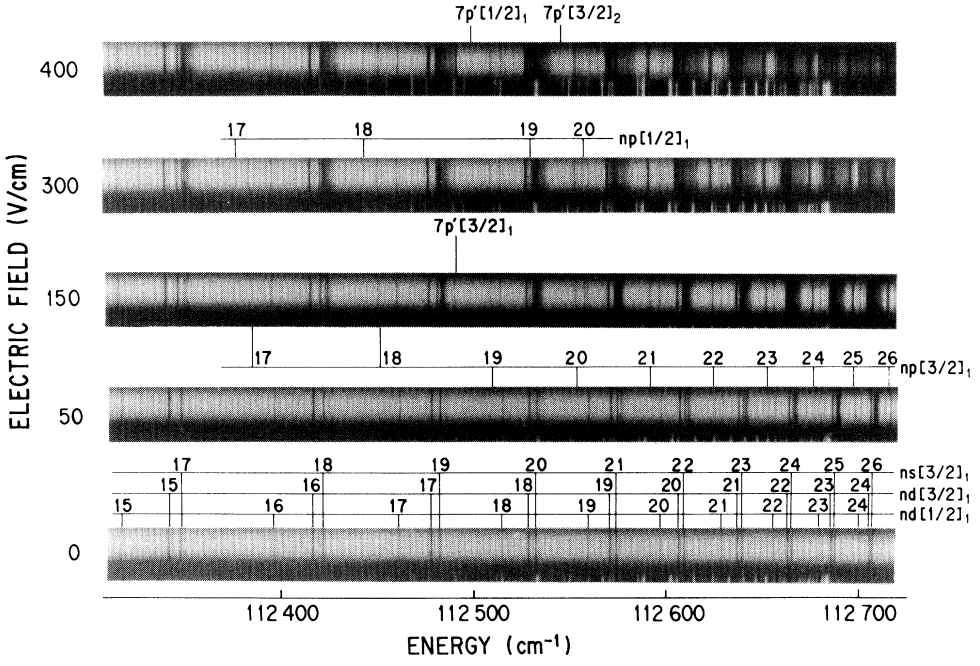

FIG. 7. Absorption spectra of Kr I at electric fields of 0–400 V/cm. The direction of the electric fields is perpendicular to the polarization of the SR.

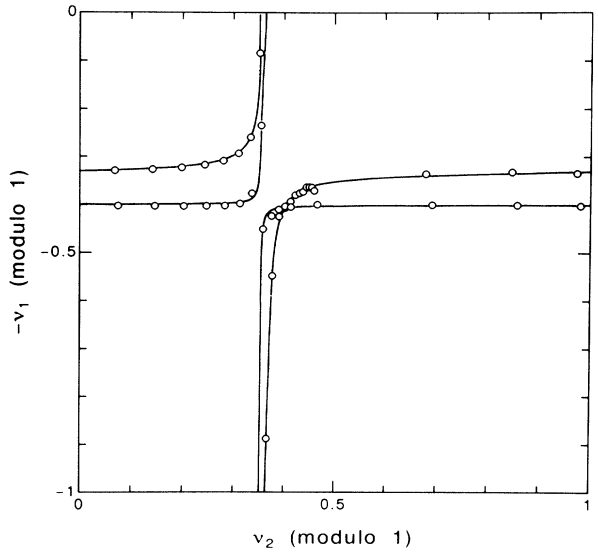

FIG. 8. Lu-Fano plots for the energy levels of the Kr I $J=1$ even parity. ○: experimental data points given in Tables III and IV; solid curves: Lu-Fano curves fitted to the data points.

els for $n \geq 19$ in Tables III and IV may be regarded as lower limits because these levels are shifted to the lower-energy side with increasing electric field The energy levels of the $7p'[1/2]_1$, $7p'[3/2]_1$, and $7p'[3/2]_2$ states obtained by extrapolation are shown in Table V with the values by Audouards *et al.* [25]. The present energy levels are in good agreement with those by Audouards *et al.*

A Lu-Fano plot for the $J=1$ energy levels with even parity is shown in Fig. 8. The odd-parity energy levels with $J=0,1,2,3$ have been thoroughly investigated by Aymar, Robaux, and Thomas [10] by means of MQDT. However, it has been difficult to obtain the even-parity energy levels which do not have optical dipole transition moments from the ground state. The energy levels in Tables III–V are used for Fig. 8, where the energy levels of the $np[1/2]_1$ and $np[3/2]_1$ series with $n<7$ are excluded. On the basis of the eigenchannel representation, four eigenchannels $\alpha=1,2,3,4$ are expected to have approximately *LS*-coupling features and are designed by conventional notation $^3S_1$, $^3P_1$, $^1P_1$, and $^3D_1$, respectively, wheres the four dissociation channels $i=1,2,3,4$ are expected to have *jj*-coupled features designated as $(^2P_{3/2})p_{3/2}$, $(^2P_{3/2})p_{1/2}$, $(^2P_{1/2})p_{3/2}$, and $(^2P_{1/2})p_{1/2}$, respectively. We have carried out a least-squares fit by using the MQDT formula [8,9] to the energy levels plotted in Fig. 8, neglecting the energy dependence of the eigenchannel quantum defects μ_α and the transformation matrix element $U_{i\alpha}$. The series limits used for the fitting were 112 914.49 and 118 284.6 cm^{-1} for $I_{3/2}$ and $I_{1/2}$, respectively [10]. The Rydberg constant for Kr I is 109 736.59 cm^{-1}. The resulting MQDT parameters are listed in Table VI. The coupling angles $\theta_{14}=0.172\,287$ and $\theta_{34}=0.144\,781$ were used to obtain the $U_{i\alpha}$'s in Table VI. It should be pointed out that the MQDT analyses have been carried out by Audouards *et al.* [25] on the even-parity energy levels with $J=0$, and by L'Huillier, Tang, and Lambropoulas [26] on the lower ones with $J=0$ and 2.

TABLE VII. Energy levels for the $np[5/2]_2$ and $np[3/2]_2$ series.

n	$np[5/2]_2(M=0)$	$np[5/2]_2(M=\pm1)$	$np[3/2]_2$
13	111 894.8	111 894.7	111 902.1
14	112 066.2	112 066.2	112 071.5
15	112 197.6	112 197.6	112 201.7
16	112 300.6	112 300.8	112 303.9
17	112 383.0	112 382.9	112 385.6
18	112 449.7	112 450.1	112 451.0

TABLE VIII. Energy levels for the $nd[3/2]_2$ series.

n	This work	Ref. [11]	Ref. [10]
12	111 942.3		
13	112 101.6		
14	112 224.9		
15	112 322.3	112 321.75	112 321.51
16	112 400.5	112 399.87	112 399.67
17	112 464.0	112 463.54	112 463.36
18	112 516.5	112 516.08	112 515.94

D. Energy levels of other series at zero field

The energy levels obtained in the present measurements are listed in Table VII for the $np[5/2]_2$ and $np[3/2]_2$ series. The $np[5/2]_2$ series are seen in both $M=0$ and $M=\pm1$ cases. The term values thus obtained are within experimental errors of each other.

In Table VIII, the energy levels for the $nd[3/2]_2$ series are listed together with the experimental values by Delsart, Keller, and Thomas [11] and with the theoretically predicted values by Aymar, Robaux, and Thomas [10]. The $nd[3/2]_2$ energy levels in the present measurements are systematically higher than the values of Delsart, Keller, and Thomas [11] and the predicted values by Aymar, Robaux, and Thomas [10]. However, as for the present values for the $nd[5/2]_2$ series, shown in Table IX, the systematic difference between the present values and the predicted ones is not seen, largely because of the experimental uncertainty in the extrapolation. If the spectral line of an energy level has a sufficiently strong intensity even at a low electric field and is isolated at a higher electric field, the energy level can be obtained properly by the extrapolation method. This is not the case for the energy levels listed in Tables VIII and IX.

TABLE IX. Energy levels for the $nd[5/2]_2$ series.

n	This work	Ref. [10]
12	111 956.3	112 957.02
13	112 112.8	112 113.18
14	112 234.4	112 234.10
15	112 329.7	112 329.61
16	112 407.9	112 406.36
17	112 469.3	112 468.94
18	112 520.6	112 520.65

IV. CONCLUDING REMARKS

The effect of the external field on the absorption spectra of Kr I was demonstrated experimentally in the photoionization threshold region. Most of the spectral lines, beside those in the Stark manifolds, are simulated properly with the Stark matrix diagonalization method. The term values of the Rydberg series which do not have optical dipole transition moment from the ground state of Kr I are obtained by extrapolating observed energy values to zero electric field. The MQDT parameters were derived first for the $J=1$ even-parity energy levels of Kr I using the term values obtained in the present measurements. However, a more refined theoretical treatment is needed for the analysis of the Stark manifold and of strongly perturbed spectral regions, for which the diagonalization method is of no use.

ACKNOWLEDGMENTS

The authors are grateful to Dr. T. Namioka for his encouragement during this work, and to Dr. K. Yoshino for the use of a comparator. This work has been performed under the approval of the Photon Factory Program Advisory Committee (Proposal No. 91-283).

[1] H. Beutler, Z. Phys. **93**, 177 (1935).
[2] K. Yoshino, J. Opt. Soc. Am. **60**, 1220 (1970).
[3] K. Yoshino and Y. Tanaka, J. Opt. Soc. Am. **69**, 159 (1979).
[4] K. Yoshino and D. E. Freeman, J. Opt. Soc. Am. B **2**, 1785 (1985).
[5] M. A. Baig and J. P. Connerade, J. Phys. B **17**, 1785 (1984).
[6] K. Ito, K. Ueda, T. Namioka, K. Yoshino, and Y. Morioka, J. Opt. Soc. Am. B **5**, 2006 (1988).
[7] M. J. Seaton, Rep. Prog. Phys. **46**, 167 (1983).
[8] K. T. Lu, Phys. Rev. A **4**, 579 (1971).
[9] Chia-Ming Lee and K. T. Lee, Phys. Rev. A **8**, 1241 (1973).
[10] M. Aymar, O. Robaux, and C. Thomas, J. Phys. B **14**, 4255 (1981).
[11] C. Delsart, J.-C. Keller, and C. Thomas, J. Phys. B **14**, 3355 (1981); **14**, 4241 (1981).
[12] C. E. Moore, *Atomic Energy Levels,* Natl. Bur. Stand. (U.S.) Circ. No. 467 (U.S. GPO, Washington, DC, 1952), Vol. 2.
[13] V. Kaufman and C. J. Humphreys, J. Opt. Soc. Am. **59**, 1614 (1969).
[14] M. L. Zimmerman, M. L. Littman, M. M. Kash, and D. Kleppner, Phys. Rev. A **20**, 2251 (1979).
[15] D. A. Harmin Phys. Rev. A **30**, 2413 (1984); in *Atoms in Strong Fields,* edited by C. A. Nicolaides, C. W. Clark, and M. H. Nayfeh (Plenum, New York, 1990), p. 61.
[16] K. Sakimoto, J. Phys. B **19**, 3011 (1986).
[17] W. E. Ernst, T. P. Softely, and R. N. Zare, Phys. Rev. A **37**, 4172 (1988).
[18] C. Delsart and J.-C. Keller, Phys. Rev. A **28**, 845 (1983).
[19] R. D. Knight and Liang-guo Wang, Phys. Rev. A **32**, 896 (1985).
[20] P. F. Brevet, M. Pellarin, and J. L. Vialle, Phys. Rev. A **42**, 1460 (1990).
[21] K. Ito, T. Namioka, Y. Morioka, T. Sasaki, T. Goto, K. Katayama, and M. Koike, Appl. Opt. **25**, 837 (1986).
[22] K. Ito, K. Yoshino, Y. Morioka, and T. Namioka, Phys. Scr. **36**, 88 (1987).
[23] L. Minhagen, J. Opt. Soc. Am **63**, 1185 (1973).
[24] A. R. Edmonds, J. Picart, N. Tran Minh, and R. Pullen, J. Phys. B **12**, 2781 (1979).
[25] E. Audouards, P. Laporte, J.-L. Subti, N. Damany, and M. Pellarin, Phys. Rev. A **41**, 6032 (1990).
[26] A. L'Huillier, X. Tang, and P. Lambropoulos, Phys. Rev. A **39**, 1112 (1989).
[27] B. Petersson, Ark. Fys. **27**, 317 (1964).

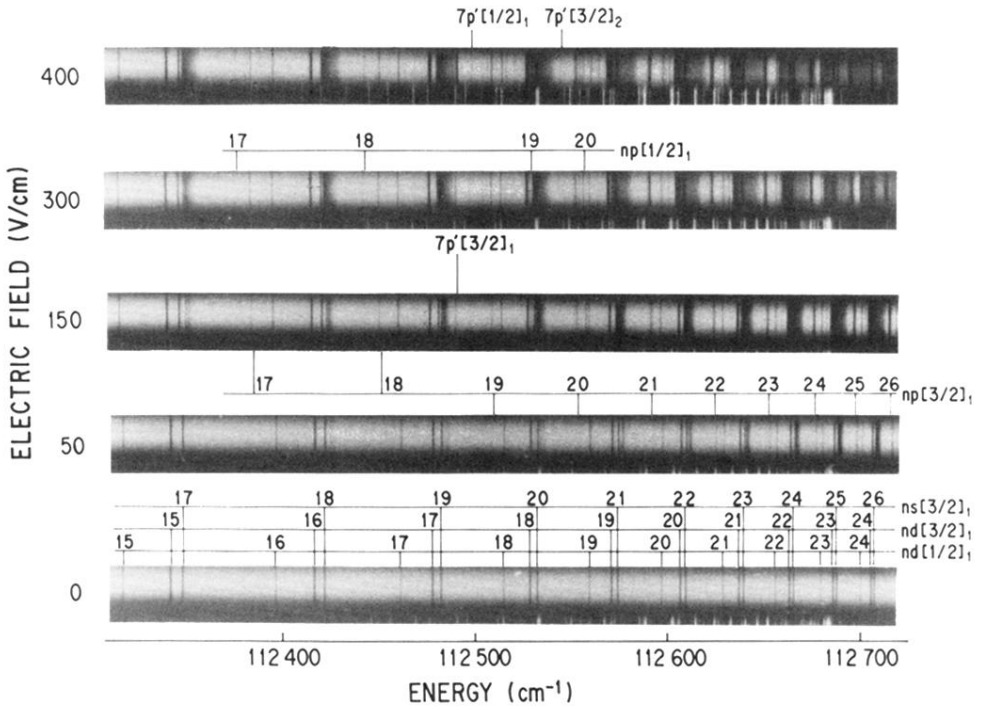

FIG. 7. Absorption spectra of Kr I at electric fields of 0–400 V/cm. The direction of the electric fields is perpendicular to the polarization of the SR.